Available online at www.sciencedirect.com
ScienceDirect
Journal of Power Sources 178 (2008) 174–180
JOURNAL OF POWER SOURCES
www.elsevier.com/locate/jpowsour

Effects of serpentine flow field with outlet channel contraction on cell performance of proton exchange membrane fuel cells

Wei-Mon Yan [a], Hung-Yi Li [a], Po-Chiao Chiu [a], Xiao-Dong Wang [b,*]

[a] *Department of Mechatronic Engineering, Huafan University, Taipei 22305, Taiwan*
[b] *Department of Thermal Engineering, School of Mechanical Engineering, University of Science & Technology Beijing, Beijing 100083, China*

Received 26 November 2007; received in revised form 5 December 2007; accepted 6 December 2007
Available online 15 December 2007

Abstract

A serpentine flow field with outlet channels having modified heights or lengths was designed to improve reactant utilization and liquid water removal in proton exchange membrane (PEM) fuel cells. A three-dimensional full-cell model was developed to analyze the effects of the contraction ratios of height and length on the cell performance. Liquid water formation, that influences the transport phenomena and cell performance, was included in the model. The predictions show that the reductions of the outlet channel flow areas increase the reactant velocities in these regions, which enhance reactant transport, reactant utilization and liquid water removal; therefore, the cell performance is improved compared with the conventional serpentine flow field. The predictions also show that the cell performance is improved by increments in the length of the reduced flow area, besides greater decrements in the outlet flow area. If the power losses due to pressure drops are not considered, the cell performance with the contracted outlet channel flow areas continues to improve as the outlet flow areas are reduced and the lengths of the reduced flow areas are increased. When the pressure losses are also taken into account, the optimal performance is obtained at a height contraction ratio of 0.4 and a length contraction ratio of 0.4 in the present design.

Keywords: Proton exchange membrane fuel cell; Channel contraction; Serpentine flow field

1. Introduction

Proton exchange membrane fuel cells (PEMFCs) are attracting considerable interests as transport, stationary and portable power sources. Modeling and simulations are being used extensively in research institutions and industries across the world to gain a better understanding of the fundamental processes, so that the design cycle can be shortened significantly. During the past decades, many analyses, models and numerical simulations have been developed [1–14] to study various transport phenomena and electrochemical kinetics, thus to gain a better understanding and to develop strategies for optimal design and operation scenarios.

Springer et al. [1] presented a one-dimensional steady-state model for a PEMFC based on experimentally determined transport parameters. Bernardi and Verbrugge [2,3] developed a full-cell model to investigate the mechanisms of water transport. Fuller and Newman [4] and Nguyen and White [5] proposed two-dimensional transport models to examine the water management problems in a PEMFC. Ge and Yi [6] developed a two-dimensional model to investigate the effects of operating conditions and membrane thicknesses on the water transport. Okada et al. [7] studied the water transport at the anode side and gave a linear transport equation based on the water diffusion and electro-osmotic water drag to analyze the water concentration profiles. Gurau et al. [8] considered the variations of the concentrations and the partial pressures in the gas channels and developed a two-dimensional model for the entire sandwich of a PEMFC. They further derived a half-cell model for the cathode side and obtained rigorous analytical solutions which account for the liquid water content in the gas diffusion layer (GDL) [9]. Um et al. [10] developed a multi-dimensional model to study the electrochemical kinetics, current distributions, fuel and oxidant flows, and multi-component transport in a PEMFC with

* Corresponding author. Tel.: +86 10 62321277; fax: +86 10 81765088.
E-mail address: wangxd99@gmail.com (X.-D. Wang).

0378-7753/$ – see front matter © 2007 Elsevier B.V. All rights reserved.
doi:10.1016/j.jpowsour.2007.12.017

an interdigitated flow field. Djilali and Lu [11] focused on the modeling of non-isothermal and non-isobaric effects to analyze the cell performance and water transport over a range of operating current densities. A quasi-three-dimensional model of water transport in PEMFCs was proposed by Kulikovsky [12] to analyze the non-linear diffusion of liquid water in the membrane. Mazumder and Cole [13,14] developed a three-dimensional model to investigate the cell performance of PEMFCs with consideration of the liquid water effects.

The flow field design in the bipolar plates of a fuel cell is one of the most important issues for a PEMFC. An appropriate flow field design in the bipolar plates can improve the reactant transport, the thermal and water management. To this end, different flow field configurations, including parallel, serpentine, interdigitated, and many other combined versions, have been developed. Many efforts have been devoted to optimize the flow field design to improve cell performance [15–38].

Recently, Soong et al. [39] proposed a relatively novel configuration of partially blocked reactant channels. They focused on the blockage effects of various gap ratios and numbers of baffles on the reactant transport and the pressure losses. They found that reducing the gap size and/or increasing the number of baffles enhanced the reactant transport. Liu et al. [40] developed a two-dimensional model to examine the reactant transport and the cell performance of a PEMFC with a tapered parallel flow channel. Numerical predictions show that the cell performance is enhanced by the tapered reactant channel, and the enhancement is more evident at lower voltages. Later, Yan et al. [41] proposed a parallel flow channel design with tapered heights or widths to improve reactant utilization efficiency for PEMFCs. A three-dimensional numerical model predicted that with the tapered channel designs, the flow area contraction along the flow channel leads to increased reactant velocities; thus, enhancing the reactant transport through the porous layers, reactant utilization and liquid water removal. The results also show that the cell performance can be improved by either decreasing the height taper ratio or increasing the width taper ratio. However, these investigations utilized simplified two-dimensional models, or only considered essential parts of the fuel cell in the computational domain to reduce the computational times. In addition, these investigations only considered the effect of tapered flow channels on the parallel flow field, while the effect on a serpentine flow field has not yet been analyzed in the available literature. This work presents an analysis of a novel serpentine flow field design with reduced outlet channel heights or lengths to improve the efficiency of reactant transport, reactant utilization, and cell performance in PEMFCs. A three-dimensional, full-cell model was developed to analyze the effect of the outlet channel height or length reductions on the cell performance and reactant transport. The effects of liquid water formation on the reactant transport were taken into account in the model. The oxygen mass flow rates and the liquid water distributions at the interface between the cathode GDL and the catalyst layer (CL), and the local current densities are analyzed to show the advantages of the channel size reductions.

2. Numerical model

Fig. 1 presents schematics of the three-dimensional PEMFCs considered in the present paper. The cell included the anode flow channels, membrane electrode assembly (including the anode GDL, anode CL, proton exchange membrane (PEM), cathode CL, and cathode GDL), and cathode flow channels. The cell has a dimension of 23 mm × 23 mm × 2.645 mm, the diffusion layer is 0.3 mm thick, the CL is 0.005 mm thick, and the PEM is 0.035 mm thick. The widths and heights of the channels and ribs are all 1 mm.

This paper analyses the effects of the reduced outlet channel sizes on the cell performance and reactant transport. The height contraction ratio of the outlet channel, δ_H, is defined as $\delta_H = H_c/H_0$, and the length contraction ratio of the outlet channel, δ_L, is defined as $\delta_L = L_c/L_0$ (as shown in Fig. 2), where H_c is the reduced height of the outlet channel, H_0 is the height of the inlet channel (1 mm), L_c is the length of the reduced part of the outlet channel, and L_0 is the total length of the channel (70.1 mm).

For convenience of comparison, the operating conditions were all the same for all the cells. The fuel cell temperature was assumed to be 323 K, the reactants on the anode side were hydrogen and water vapor with a relative humidity of 100%, while the reactants on the cathode side were oxygen, nitrogen, and water vapor with a relative humidity of 100%, the inlet flow rate on the anode side was 150 $cm^3\ min^{-1}$, and the inlet flow rate on the cathode side was 300 $cm^3\ min^{-1}$.

A three-dimensional full-cell model was developed to analyze the electrochemical reactions, the transport phenomena of the reactants and the products in the cell using the finite volume method. The governing equations include the mass, momentum, species and electrical potential conservation equations. The model assumes that the system is three-dimensional and steady; the inlet reactants are ideal gases; the system is isothermal; the flow is laminar; the fluid is incompressible; the thermophysical properties of the reactants and products are constant; and the porous layers such as the diffusion layer, the CL and the PEM are isotropic. More details on the numerical model and solution procedure were given elsewhere [39–42]. All the parameters used in the model are listed in Table 1.

3. Results and discussion

The grid independence was examined in the preliminary test runs. Three non-uniformly distributed grid configurations were evaluated for a PEMFC with $\delta_H = 0.4$ and $\delta_L = 0.3$ at an operating voltage of 0.3 V. The numbers of elements in the X, Y and Z directions were: (I) 93 × 93 × 42, (II) 116 × 116 × 48 and (III) 139 × 139 × 54. The influence of the elements number on the local current density is shown in Fig. 3. The variation of local current densities was 5.82–12.89% for grids (I) and (II), and only 0.76–2.71% for grids (II) and (III). Thus, grid (II) was chosen as a tradeoff between accuracy and execution time in the simulations.

In the present paper, the oxygen mass flow rates, the liquid water distributions, and the local current densities on the spe-

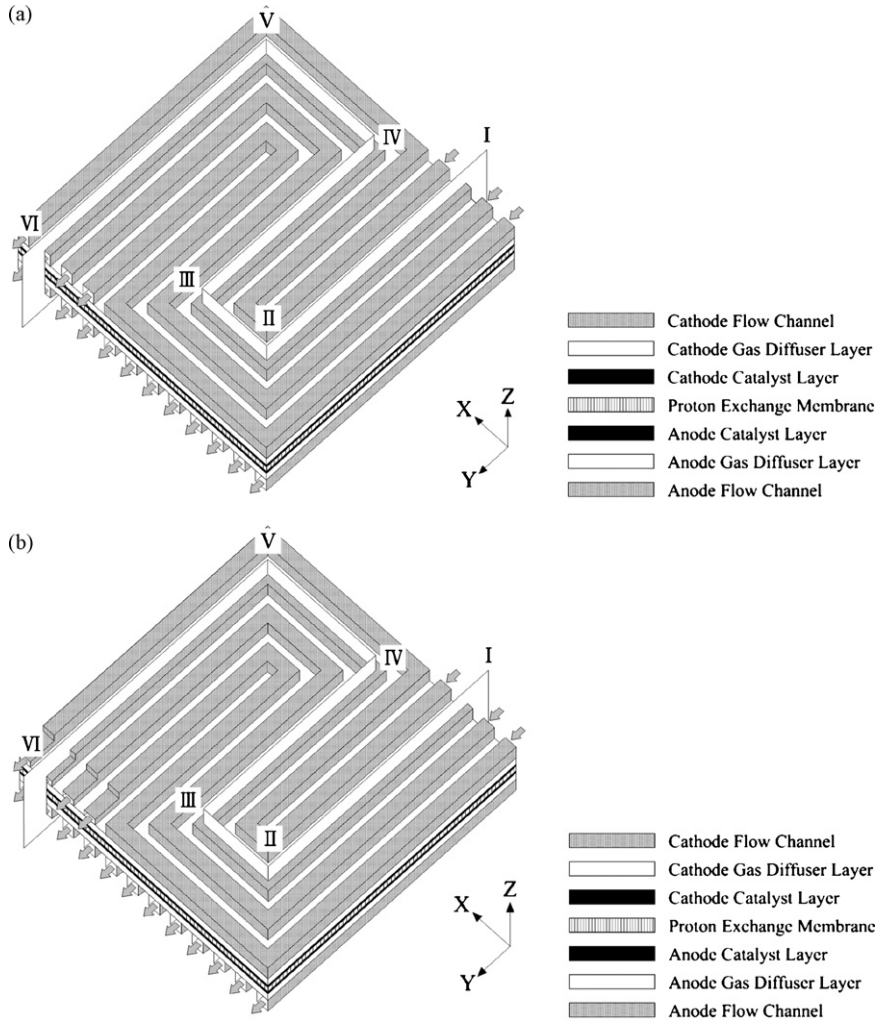

Location	I Inlet	II 1st Turn	III 2nd Turn	IV 3rd Turn	V 4th Turn	VI Outlet
L (mm)	0	18.5	24.5	40.5	50.5	71

Fig. 1. Schematics of PEMFCs. (a) Conventional serpentine flow field and (b) serpentine flow field with contracted outlet channels.

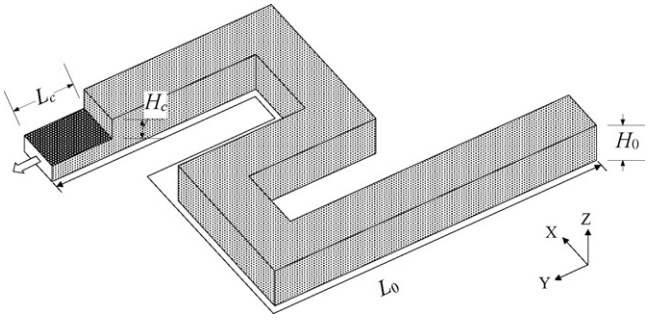

Fig. 2. Schematic of single serpentine flow channel with contracted outlet channel height and length.

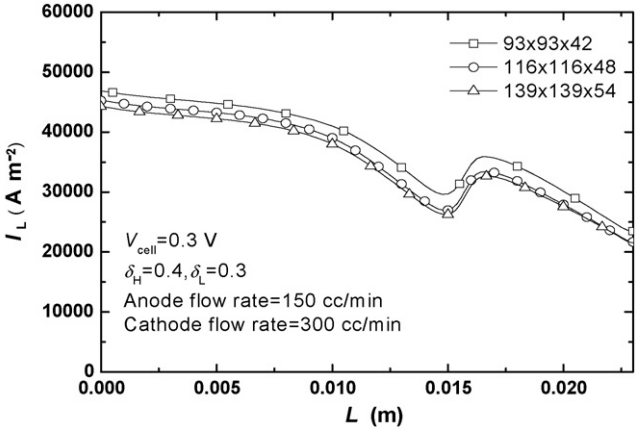

Fig. 3. Influence of the number of grid elements on the local current densities at an operating voltage of 0.3 V.

Table 1
Fuel cell parameters

Parameter	Value
$Aj_{0,a}^{ref}$	9.23×10^8 A m^{-3}
$Aj_{0,c}^{ref}$	1.5×10^2 A m^{-3}
α_a	0.5
α_c	1.5
$\varepsilon_{channel}$	1
$\tau_{channel}$	1
$k_{channel}$	∞ m^2
ε_{GDL}	0.4
τ_{GDL}	1.5
k_{GDL}	1.76×10^{-11} m^2
ε_{CL}	0.4
τ_{CL}	1.5
k_{CL}	1.76×10^{-11} m^2
ε_{Mem}	0.28
τ_{Mem}	Dagan model
k_{Mem}	1.8×10^{-18} m^2

cified cross-sections inside the cell at the two representative operating voltages of 0.3 V and 0.7 V, as shown in Fig. 1, were analyzed to understand the effects of the various flow field designs on the cell performance. The oxygen mass flow rates and liquid water distributions were analyzed at the interface between the cathode GDL and the CL, with the local current densities analyzed at the middle cross-section of the PEM. The local transport phenomena in the entire cell were analyzed by plotting all local physical quantities along a specified serpentine channel (Fig. 1) from the inlet to the outlet.

3.1. Effect of outlet channel height contraction ratio

The effect of the outlet channel height contraction ratio on the cell performance was analyzed at δ_H equal to 0.2, 0.4 0.6 and 0.8 with a fixed $\delta_L = 0.3$. The conventional serpentine flow field (without contractions) was used as the baseline.

Fig. 4 shows the effect of δ_H on the local oxygen mass flow rates through the cathode GDL–CL interface at operating voltages of 0.3 V and 0.7 V, where L denotes the distance from the flow channel inlet. Fig. 4 indicates that at the higher operating voltage of 0.7 V, the oxygen mass flow rates are almost unchanged along the flow direction and are almost equal for the five designs. At the lower operating voltage of 0.3 V, the oxygen mass flow rates are all higher than those at the higher operating voltage of 0.7 V for the five designs, indicating that at lower operating voltages the electrochemical reactions are stronger with more oxygen consumption. For all five designs, the maximum oxygen mass flow rates occur at the inlet and gradually decrease along the flow directions, with local maximums at the turns in the flow channels (L = 18.5 mm, 24.5 mm, 40.5 mm and 50.5 mm as shown in Fig. 1). The inlet oxygen concentration is the highest, thus the largest oxygen mass flow rates through the GDL–CL interface occur near the inlet. Then, the oxygen is gradually consumed by the electrochemical reaction, so the oxygen concentration gradually decreases along the flow direction, and thus, the oxygen mass flow rate across the GDL–CL interface gradually decreases. At the channel turns, the corners of flow channels force more reactants to flow into the GDL and CL, thus, the oxygen mass flow rates through the GDL–CL interface sharply increase at the turns. Fig. 4 also indicates that the local oxygen mass flow rates oscillate in the transverse flow channels (L = 18.5–24.5 mm and L = 40.5–50.5 mm) because the anode flow field channels are in parallel. Furthermore, near the flow channel outlets, where the flow channel cross-sectional area reduces, as δ_H increases the flow channel area decreases and the reactant flow velocities increase, which improves the liquid water removal efficiency, so the local oxygen mass flow rates increase.

Fig. 5 shows the effect of δ_H on the liquid water concentrations along the cathode GDL–CL interface at operating voltages of 0.3 V and 0.7 V. Fig. 5 indicates that for the five designs the liquid water concentrations at 0.3 V operating voltage are all higher than those at 0.7 V operating voltage due to the higher electrochemical reaction rates. At the lower operating voltage of 0.3 V, the liquid water concentrations gradually increase along the flow directions, with local minimums at the turns in the flow channels (L = 18.5 mm, 24.5 mm, 40.5 mm and 50.5 mm). In addition, the liquid water concentrations also oscillate in the transverse flow channel (L = 18.5–24.5 mm and

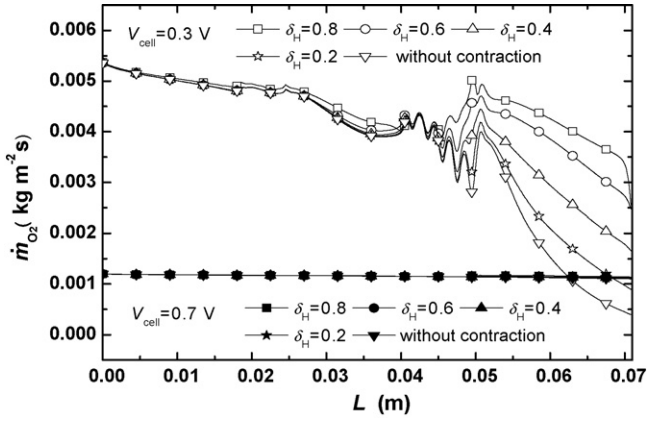

Fig. 4. Oxygen mass flow rates on the cathode GDL–CL interface for various δ_H with fixed δ_L = 0.3 at operating voltages of 0.3 V and 0.7 V.

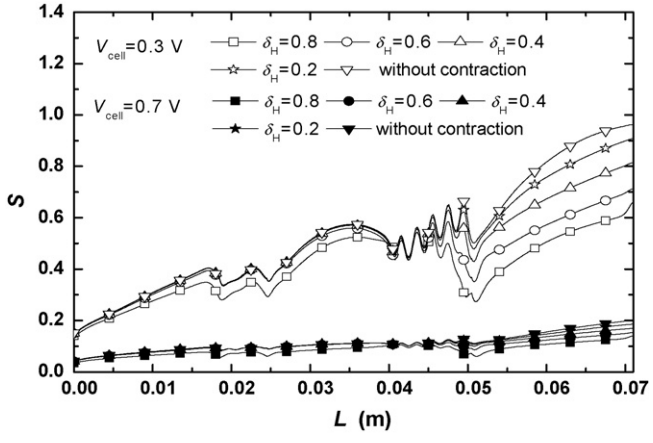

Fig. 5. Liquid water distributions on the cathode GDL–CL interface for various δ_H with fixed δ_L = 0.3 at operating voltages of 0.3 V and 0.7 V.

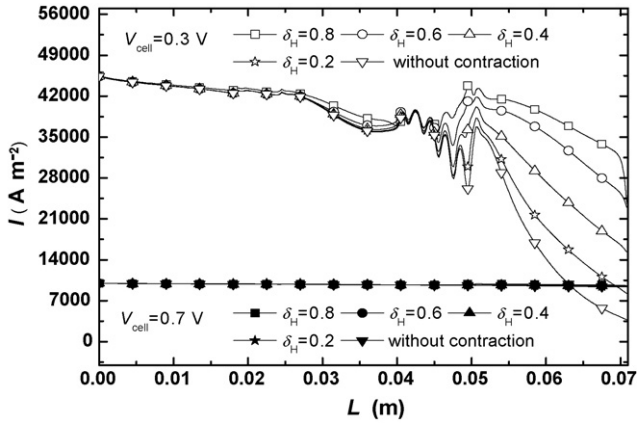

Fig. 6. Local current densities on the middle cross-section in the PEM for various δ_H with fixed $\delta_L = 0.3$ at operating voltages of 0.3 V and 0.7 V.

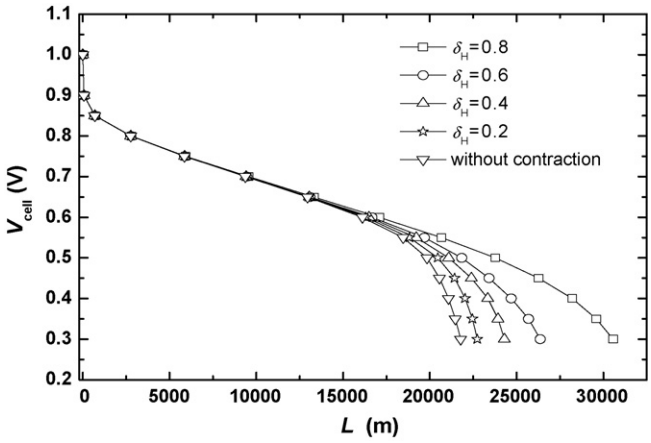

Fig. 8. Polarization curves of PEMFCs for various δ_H with a fixed $\delta_L = 0.3$.

$L = 40.5$–50.5 mm) because the anode flow channels are in parallel. Fig. 5 also indicates that the reduced height outlet channel heights efficiently improve the removal of liquid water trapped in the porous layers. As δ_H increases, the reactant flow velocities increase and the liquid water removal efficiency increases.

Fig. 6 shows the effect of δ_H on the local current densities of the middle cross-section in the PEM at operating voltages of 0.3 V and 0.7 V. A comparison of Figs. 4–6 indicates that the local current density distributions are similar to the oxygen mass flow rate distributions, but are opposite to the liquid water concentration distributions. This is because lower liquid water concentrations at the cathode GDL–CL interface allow more oxygen to enter the CL to participate in the electrochemical reactions, so the oxygen flow rates and the local current densities increase.

The flow field design affects not only the cell performance but also the pressure drop in the fuel cell. Large pressure drops in the fuel cell mean that more power is needed to pump the reactants. Thus, the pressure drop is a significant issue to be considered in choosing the flow field designs besides the I–V_{cell} curve. Fig. 7 shows the effect of δ_H on the local pressure drops on the middle cross-section in the flow channels at voltages of 0.3 V and 0.7 V. Fig. 7 shows that the operating voltage has relatively small effect on the pressure drops. At the lower operating voltage of 0.3 V, the pressure drops are slightly higher than at the higher operating voltage of 0.7 V because more liquid water is produced and accumulated in the porous layer and the flow channels, which increases the flow resistances. However, as δ_H increases, the pressure drops increase sharply because the decrement of the flow channel cross-sectional areas and increment of the flow resistances. For example, the total pressure drop for $\delta_H = 0.6$ is about three times higher than that of the conventional serpentine flow field, while for $\delta_H = 0.8$ it becomes about eleven times higher than that of the conventional serpentine flow field.

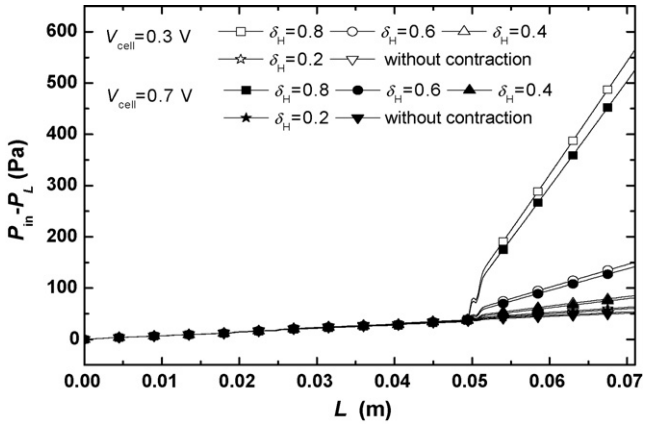

Fig. 7. Pressure drops on the middle cross-section in the flow channel for various δ_H with a fixed $\delta_L = 0.3$ at operating voltages of 0.3 V and 0.7 V.

Fig. 8 shows the I–V_{cell} polarization curves for the various δ_H. Fig. 8 indicates that at high operating voltages, the cell performance is not dependent on the flow channel design, while at low operating voltages the cell performance is significantly affected by the flow channel design. As δ_H increases, the limiting current density increases and the cell performance improves. Although larger outlet channel height contraction ratios improve the cell performance, the contractions also significantly increase the pressure drops; therefore, there is an optimal height contraction ratio. With the present design, the optimal cell performance occurs at $\delta_H = 0.4$.

3.2. Effect of the outlet channel length contraction ratio

The effect of the outlet channel length contraction ratio on the cell performance was analyzed at δ_L equal to 0.1, 0.2 0.3 and 0.4 with a fixed $\delta_H = 0.4$. Again, the conventional serpentine flow field was used as the baseline.

Fig. 9 shows the effect of δ_L on the local oxygen mass flow rates through the cathode GDL–CL interface at operating voltages of 0.3 V and 0.7 V. Fig. 9 shows that the oxygen mass flow rates at 0.3 V is much larger than those at 0.7 V, indicating that the electrochemical reactions are stronger with more liquid water produced. In addition, the oxygen mass flow rates along the flow direction distribute quite unevenly, so that the flow field designs significantly affect the cell performance at low operating voltages. Fig. 9 also shows that at the lower operating voltage of 0.3 V, the distributions of the oxygen mass

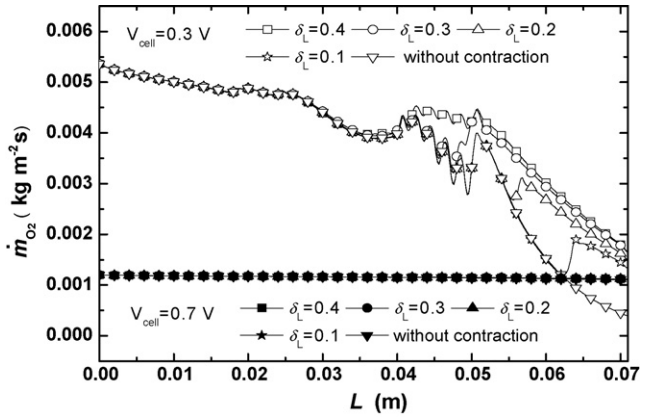

Fig. 9. Oxygen mass flow rates on the cathode GDL–CL interface for various δ_L with fixed $\delta_H = 0.4$ at operating voltages of 0.3 V and 0.7 V.

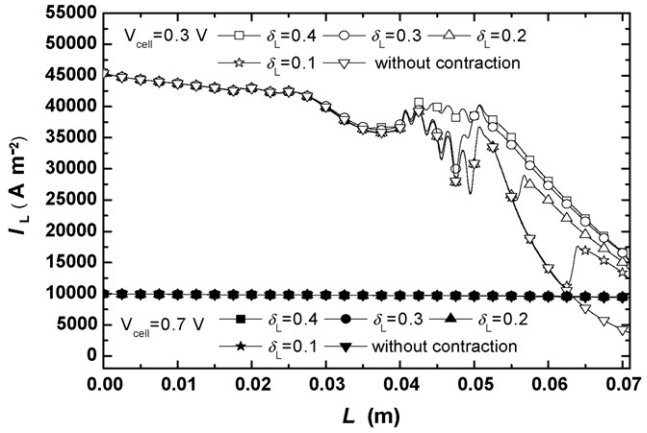

Fig. 11. Local current densities on the middle cross-section in the PEM for various δ_L with fixed $\delta_H = 0.4$ at operating voltages of 0.3 V and 0.7 V.

flow rates almost coincide at $L < 0.0426$ m for all the five designs, because the flow channel does not start to contract until $L = 0.0426$ m. At $L > 0.0426$ m, the oxygen mass flow rates for $\delta_L = 0.4$ increase due to the higher reactant flow velocity. Similarly, at $L = 0.0497$ m for $\delta_L = 0.3$, $L = 0.0568$ m for $\delta_L = 0.2$, and $L = 0.0639$ m for $\delta_L = 0.1$, the oxygen mass flow rates start to increase. Therefore, the contracted region of the outlet channels increase as δ_L increases, and the oxygen utilization efficiency is enhanced.

Fig. 10 shows the effect of δ_L on the liquid water concentrations along the cathode GDL–CL interface at operating voltages of 0.3 V and 0.7 V. Fig. 10 indicates that at the higher operating voltage of 0.7 V, the liquid water concentrations for all the five designs are lower than those at the lower operating voltage of 0.3 V due to the weaker electrochemical reaction rates. The liquid water concentrations gradually increase along the flow directions and almost coincide at $L < 0.0426$ m for the five designs. At $L = 0.0426$ m, where the flow channel starts to contract for $\delta_L = 0.4$, the reactant flow velocity significantly increases, which enhances the liquid water removal, so the liquid water concentration for $\delta_L = 0.4$ is lower than those for the other four designs. Similarly, at $L = 0.0497$ m for $\delta_L = 0.3$, $L = 0.0568$ m for $\delta_L = 0.2$, and $L = 0.0639$ m for $\delta_L = 0.1$, the liquid water concentrations start to decrease. Therefore, as δ_L increases, which means longer flow channel contractions, the liquid water removal efficiency enhances.

Fig. 11 shows the effect of δ_L on the local current densities at the middle cross-section of the PEM with operating voltages of 0.3 V and 0.7 V. A comparison of Figs. 9–11 again indicates that the local current density distributions are similar to the oxygen mass flow rate distributions, but are opposite to the liquid water concentration distributions. Therefore, increasing δ_L improves cell performance due to the higher oxygen mass flow rates and the lower liquid water concentrations in the porous layers under the contracted outlet channels.

Fig. 12 shows the effect of δ_L on the local pressure drops at the middle cross-section of the flow channels with voltages of 0.3 V and 0.7 V. Fig. 12 indicates that although the increments of δ_L promote the pressure drops, the amount of pressure drops are very small compared to those caused by increments of δ_H. For example, the pressure drop is 95.1 Pa for $\delta_L = 0.4$, 85.4 Pa for $\delta_L = 0.3$, 75.1 Pa for $\delta_L = 0.2$ and 66.6 Pa for $\delta_L = 0.1$, with increments of only 76.1% for $\delta_L = 0.4$, 58.1% for $\delta_L = 0.3$, 39.1% for $\delta_L = 0.2$ and 23.3% for $\delta_L = 0.1$, compared to 54.0 Pa for the conventional serpentine flow field design.

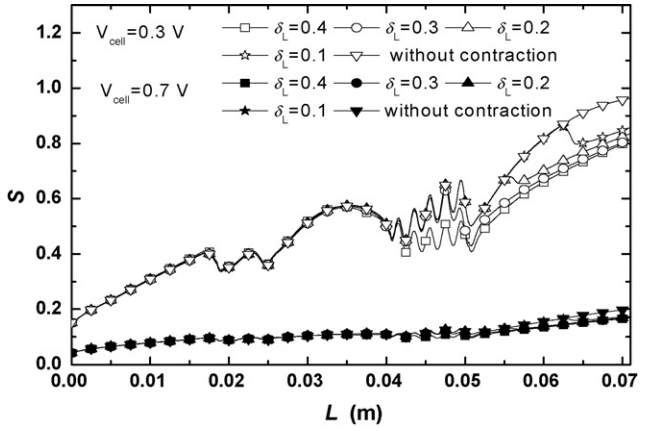

Fig. 10. Liquid water distributions on the cathode GDL–CL interface for various δ_L with fixed $\delta_H = 0.4$ at operating voltages of 0.3 V and 0.7 V.

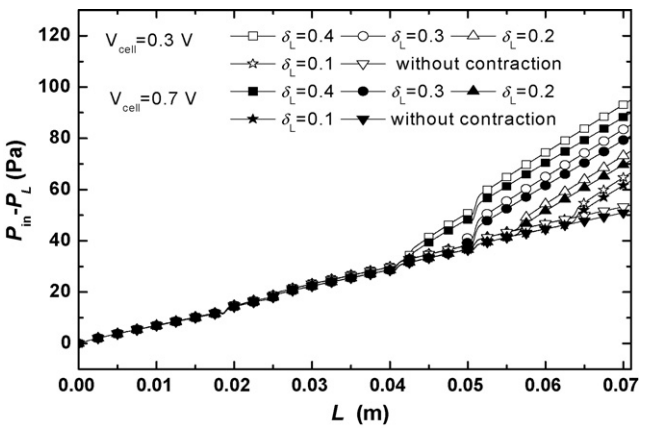

Fig. 12. Pressure drops on the middle cross-section in the flow channel for various δ_L with a fixed $\delta_H = 0.4$ at operating voltages of 0.3 V and 0.7 V.

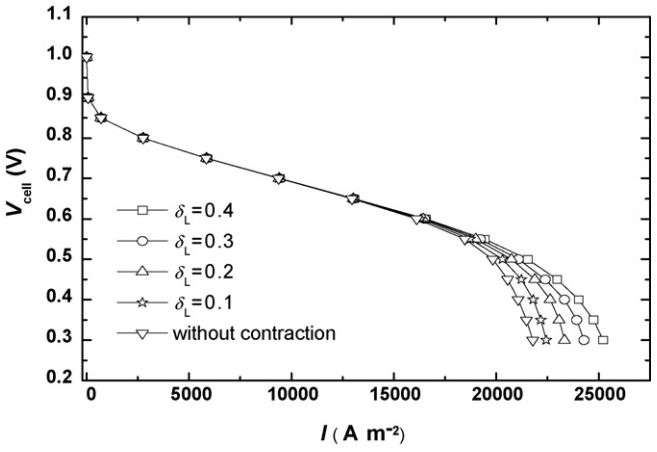

Fig. 13. Polarization curves of PEMFCs for various δ_L with a fixed $\delta_H = 0.4$.

Fig. 13 shows the I–V_{cell} polarization curves for the various δ_L, which indicates that as δ_L increases, the limiting current density increases and the cell performance improves because larger δ_L means longer contraction areas in the outlet channels, which enhances the oxygen utilization and the liquid water removal. Because increments in the outlet channel length contraction ratios only slightly increase the pressure drop, the optimal cell performance occurs at $\delta_L = 0.4$ with the present design.

4. Conclusions

A three-dimensional numerical model was used to examine the effects of reductions of the outlet channel flow area on cell performance and local transport phenomena. The conclusions drawn from the analyses are:

(1) For operating voltages greater than 0.7 V, the electrochemical reaction rates are lower with less oxygen consumption and less liquid water production, then the cell performance is not dependent on the flow channel design. However, for lower operating voltages, the electrochemical reaction rates gradually increase as the operating voltage decreases. The oxygen transport capability and the liquid water removal efficiency then differ for the various flow fields; therefore, the cell performance is strongly dependent on the flow field design.
(2) With a fixed $\delta_L = 0.3$, larger δ_H causes the reactant velocities in the contracted outlet channels to increase significantly, which enhances liquid water removal and oxygen transport, as a result, the cell performance is significantly improved. Taking the pressure drop into account, the optimal performance occurs at $\delta_H = 0.4$ in this design.
(3) With a fixed $\delta_H = 0.4$, larger δ_L increases the outlet channel contraction region, enhances the oxygen mass flow rates and the liquid water removal efficiency significantly, so the cell performance improves.

Acknowledgement

This study was supported by the National Science Council through grant number NSC 94-2212-E-211-004.

References

[1] T.E. Springer, T.A. Zawodzinski, S. Gottesfeld, J. Electrochem. Soc. 138 (1991) 2334.
[2] D.M. Bernardi, M.W. Verbrugge, AIChE J. 37 (1991) 1151.
[3] D.M. Bernardi, M.W. Verbrugge, J. Electrochem. Soc. 139 (1992) 2477.
[4] T.F. Fuller, J. Newman, J. Electrochem. Soc. 140 (1993) 1218.
[5] T.V. Nguyen, R.E. White, J. Electrochem. Soc. 140 (1993) 2178.
[6] S.H. Ge, B.L. Yi, J. Power Sources 124 (2003) 1.
[7] T. Okada, G. Xie, Y. Tanabe, J. Electroanal. Chem. 413 (1996) 49.
[8] V. Gurau, H. Liu, S. Kakac, AIChE J. 44 (1998) 2410.
[9] V. Gurau, F. Barbir, H. Liu, J. Electrochem. Soc. 147 (2000) 2468.
[10] S. Um, C.Y. Wang, K.S. Chen, J. Electrochem. Soc. 147 (2000) 4485.
[11] N. Djilali, D. Lu, Int. J. Therm. Sci. 41 (2002) 29.
[12] A.A. Kulikovsky, J. Electrochem. Soc. 150 (2003) A1432.
[13] S. Mazumder, J.V. Cole, J. Electrochem. Soc. 150 (2003) A1503–A1509.
[14] S. Mazumder, J.V. Cole, J. Electrochem. Soc. 150 (2003) A1510–A1517.
[15] T.V. Nguyen, J. Electrochem. Soc. 143 (1996) L103.
[16] S.W. Cha, R.O. Hayre, Y. Saito, F.B. Prinz, J. Power Sources 124 (2004) 57.
[17] S.W. Cha, R. O'Hayre, S.J. Lee, Y. Saito, F.B. Prinz, J. Electrochem. Soc. 151 (2004) 1856.
[18] M.V. Williams, H.R. Kunz, J.M. Fenton, J. Electrochem. Soc. 151 (2004) A1617.
[19] W.M. Yan, C.Y. Soong, F.L. Chen, H.S. Chu, J. Power Sources 143 (2005) 48.
[20] H.C. Liu, W.M. Yan, C.Y. Soong, F.L. Chen, J. Power Sources 142 (2005) 125.
[21] F.B. Weng, A. Su, C.Y. Hsu, C.Y. Lee, J. Power Sources 157 (2006) 674.
[22] J. Scholta, F. Häussler, W. Zhang, L. Kuppers, L. Jörissen, W. Lehnert, J. Power Sources 155 (2006) 60.
[23] Y. Wang, C.Y. Wang, J. Power Sources 153 (2006) 130.
[24] L. Sun, P.H. Oosthuizen, K.B. McAuley, Int. J. Therm. Sci. 45 (2006) 1021.
[25] S.S. Hsieh, S.H. Yang, C.L. Feng, J. Power Sources 162 (2006) 262.
[26] J.H. Jang, W.M. Yan, H.Y. Li, Y.C. Chou, J. Power Sources 159 (2006) 468.
[27] W.M. Yan, H.Y. Hung, W.C. Tsai, J. Electrochem. Soc. 153 (2006) A1984.
[28] J.P. Feser, A.K. Prasad, S.G. Advani, J. Power Sources 161 (2006) 404.
[29] S. Shimpalee, S. Greenway, J.W. Van Zee, J. Power Sources 160 (2006) 398.
[30] C. Xu, Y.L. He, T.S. Zhao, R. Chen, Q. Ye, J. Electrochem. Soc. 153 (2006) A1358.
[31] Q. Ye, T.S. Zhao, C. Xu, Electrochim. Acta 51 (2006) 5420.
[32] D.H. Ahmed, H.J. Sung, J. Power Sources 162 (2006) 327.
[33] C. Xu, T.S. Zhao, Electrochem. Commun. 9 (2007) 497.
[34] S. Shimpalee, J.W. Van Zee, Int. J. Hydrogen Energy 32 (2007) 842.
[35] X.D. Wang, Y.Y. Duan, W.M. Yan, J. Power Sources 172 (2007) 265.
[36] X.D. Wang, Y.Y. Duan, W.M. Yan, J. Power Sources 173 (2007) 210.
[37] H.C. Liu, W.M. Yan, X.D. Wang, J. Electrochem. Soc. 154 (2007) B1338.
[38] X.D. Wang, Y.Y. Duan, W.M. Yan, X.F. Peng, J. Power Sources 175 (2008) 397.
[39] C.Y. Soong, W.M. Yan, C.Y. Tseng, H.C. Liu, F.L. Chen, H.S. Chu, J. Power Sources 143 (2005) 36.
[40] H.C. Liu, W.M. Yan, C.Y. Soong, F.L. Chen, H.S. Chu, J. Power Sources 158 (2006) 78.
[41] W.M. Yan, H.C. Liu, C.Y. Soong, F.L. Chen, C.H. Cheng, J. Power Sources 161 (2006) 907.
[42] X.D. Wang, Y.Y. Duan, W.M. Yan, F.B. Weng, J. Power Sources 176 (2008) 247–258.